Identification of a Potential Inhibitor of the FIV p24 Capsid Protein and Characterization of Its Binding Site

Mathieu Long, François-Xavier Cantrelle, Xavier Robert, Emmanuelle Boll, Natalia Sierra, Patrice Gouet, Xavier Hanoulle, Guzmán I Alvarez, Christophe Guillon

Identification of a potential inhibitor of the FIV p24 capsid protein and characterization of its binding site

*Mathieu Long[1], François-Xavier Cantrelle[2,3], Xavier Robert[1], Emmanuelle Boll[2,3], Natalia Sierra[4], Patrice Gouet[1], Xavier Hanoulle[2,3], Guzmán I. Alvarez[4] *, Christophe Guillon[1] **

1- UMR 5086 - Molecular Microbiology and Structural Biochemistry, CNRS/Université Lyon 1, Lyon, France

2- CNRS, ERL9002 - Integrative Structural Biology, F-59000, Lille, France

3- Univ. Lille, INSERM, CHU Lille University Hospital, Institut Pasteur de Lille, UMR1167 - RID-AGE-Risk factors and molecular determinants of aging-related, F-59000, Lille, France

4- Laboratorio de Moléculas Bioactivas, CENUR Litoral Norte, Universidad de la República, Paysandú, Uruguay

Running title: Characterization of a FIV p24 inhibitor binding site

Keywords: Feline immunodeficiency Virus, NMR, assembly inhibitor, molecular modeling, capsid

Abstract

Feline immunodeficiency virus (FIV) is a veterinary infective agent against which there is currently no efficient drug available. Drugs targeting the lentivirus capsid are currently under development for the treatment of human immunodeficiency virus 1 (HIV-1). Here we describe a lead compound that interacts with the FIV capsid. This compound, **696**, modulates the *in vitro* assembly of and stabilizes the assembled capsid protein. To decipher the binding mechanism of this compound to the protein, we performed the first nuclear magnetic resonance (NMR) assignment of the FIV p24 capsid protein. Experimental NMR chemical shift perturbations (CSPs) observed after the addition of **696** enabled the characterization of a specific binding site for **696** on p24. This site was further analyzed by molecular modeling of the protein:compound interaction, demonstrating a strong similarity with the binding sites of existing drugs targeting the HIV-1 capsid protein. Taken together, we characterized a promising capsid-interacting compound with a low cost of synthesis, for which derivatives could lead to the development of efficient treatments for FIV infection. More generally, our strategy combining the NMR assignment of FIV p24 with NMR CSPs and molecular modeling will be useful for the analysis of future compounds targeting p24 in the quest to identify an efficient treatment for FIV.

Introduction

Feline immunodeficiency virus (FIV) is a lentivirus that can infect domestic cats and wild feline species[1,2]. Infected animals can develop an immunodeficiency syndrome similar to human acquired immunodeficiency syndrome (AIDS), which is caused by infection with human immunodeficiency virus (HIV)[1,3–5]. Since its discovery in 1987, FIV has been detected worldwide in domestic and wild feline species and up to 10% of all domestic cats are thought to be infected[2,4,6]. A commercial vaccine, only used in Northern America, Australia, New Zealand, and Japan[7], showed low efficacy

against virus infectivity, and to date, no antiviral strategy has led to the efficient control of FIV viremia in infected animals[8,9]. Hence, there is a need for the development of efficient anti-FIV drugs, which must remain economically affordable not only for domestic veterinary practice but also for FIV epidemics in endangered wild feline species[10].

In addition to its importance as a causative agent of feline AIDS, FIV has been thoroughly studied as a model of HIV-1 infection to test prophylactic and therapeutic antiretroviral drugs and vaccines[11–14]. Strategies for repositioning efficient HIV-1 treatments to tackle FIV infection have also been studied to identify treatments suitable for these veterinary needs. For instance, nucleoside analogues, such as 3'-azido-3'-deoxythymidine (AZT), have been tested as treatments of FIV infection[15–17]. However, none have proven to have sufficient treatment efficacy against FIV[8,17]. Therefore, FIV must be studied specifically to develop targeted treatments for use in veterinary medicine.

Lentiviruses are enveloped viruses that are characterized by a protein-based matrix below the membrane that protects the viral capsid containing the genome. The lentivirus genome is composed of a dimer of gRNA complexed with the nucleocapsid[18–21]. Lentiviral Gag and Gag-Pol polyproteins assemble at the membrane to form immature, noninfectious viral particles (HIV-1 Gag and FIV Gag: UniProtKB **P04591** and **P16087**, respectively). This assembly occurs via the homotypic multimerization of the Gag polyprotein through its p24 region[19,22] to stabilize the Gag-RNA complexes[23] during gRNA encapsidation. After virus budding, the Gag polyproteins are cleaved by the viral protease, and several mature subunits are released, including the p24 subunit[20], which then reorganize to generate the mature, infectious viral particles. The lentiviral capsid is composed of 1,500 to 5,000 copies of the p24 protein[23–27]. HIV-1 p24 protein has been shown to form hexamers and pentamers (capsomers) that subsequently assemble as a pseudo-icosahedral,

fullerene-shaped capsid core[28]. The same fullerene-shaped core is observed in FIV, suggesting that FIV p24 assembly is similar to that of HIV-1 p24[29]. Thus, p24 assembly appears to be a key step in the maturation of infectious FIV particles and thus in the FIV life cycle.

In addition to its role in the production of infectious virions, p24 assembly is critical for the post-entry processes of the lentivirus life cycle. Indeed, the viral capsid of HIV-1 has been shown to be required for the early stages of infection of a new cell, including the entry of the viral genome into the nucleus and reverse transcription[30–33]. The reverse transcription stage occurs inside the viral capsid, transforming the gRNA into a double-stranded viral DNA (dsDNA)[30,34]. The capsid is transported to the nucleus via the cytoskeleton[35–37]. During its intracytoplasmic transport, the capsid must avoid the host cell's restriction factors. In lentiviruses, this escape is mediated by the interaction of lentiviral p24 proteins with cellular cyclophilin A (CypA, UniProtKB: **P62937**)[38]. Capsid disassembly is then required for the efficient release of the viral dsDNA and its integration into the host cell's genome. While it is not completely clear whether this uncoating occurs in the nucleus or in the cytoplasm, recent experiments have revealed the presence of the capsid inside the nucleus[30,34,39,40]. The HIV-1 p24 subunit is also involved in interactions with other cellular proteins, such as nucleoporins Nup153 and Nup358 and the cleavage and polyadenylation specificity factor subunit 6 (CPSF-6)[41–44,33] (hNup153, hNup358, and hCPSF6: UniProtKB **P49790**, **P49792**, and **Q16630**, respectively). These cellular proteins are involved in both the transport of the capsid from the basal membrane to the nucleus and nuclear import. Therapeutic drugs targeting the capsid have been developed for their ability to impair the assembly process, prevent interactions with cellular partners required for HIV-1 infectivity, or prevent capsid uncoating[45–49].

In HIV-1, most mutations that affect the structure or stability of HIV-1 p24 assembly decrease infectivity[50]. Hence, drugs targeting the capsid seem promising as efficient treatments due to the limited adaptive capacities of p24. Therefore, compounds inhibiting the assembly, uncoating, and/or interactions between the capsid and the above-mentioned cellular partners are currently under study for their impact on HIV-1 infectivity, for example, PF74 and its derivatives, which target the nucleoporin- or CPSF-6-binding sites[33,41,49,51,52].

Currently, there are no effective drugs to treat FIV[5]. Moreover, reference compounds targeting HIV-1 assembly, such as PF74, do not inhibit FIV replication *in vitro*[53]. However, the identification of compounds inhibiting the function of FIV p24 is still anticipated. To identify molecules that interfere with FIV p24 capsid assembly, we performed *in vitro* assembly assays and screened approximately 400 compounds from our in-house chemical library, as previously described[54]. This screening led to the identification of one promising lead compound, **696**. Microscale thermophoresis (MST) results revealed that **696** specifically binds p24, whose binding site was identified at the molecular level using liquid-state nuclear magnetic resonance (NMR) spectroscopy. To this purpose, we performed the first NMR resonance assignments of FIV p24 and then conducted chemical shift perturbation (CSP) experiments to characterize the binding site for **696** on p24. These experimental data were used to model the interaction between **696** and FIV p24 through molecular docking experiments. This model suggested a stabilizing role for **696** on FIV p24 assembly, which we were able to demonstrate *in vitro*. Taken together, this characterization of compound **696** paves the way for the identification of additional FIV capsid inhibitors that could ultimately lead to the development of an anti-FIV drug.

Materials and methods

Unlabeled protein production. Bacterial lysis, protein purification, and tag removal were performed using the full-length FIV p24 vector, as described earlier[29], except that the storage buffer was phosphate buffer (pH 6.8) containing 50 mM NaCl.

***In vitro* assembly/disassembly assay.** The assembly of p24 was performed and monitored, as previously described[54]. Assembly was triggered using a 1:1 (v/v) mix of 7 mg/mL purified protein in 50 mM NaPi buffer pH 7.4 containing 1M NaCl in a final volume of 50 µL. The optical density at 345 nm was measured every 40 sec using the Infinite M1000 multiplate reader (Tecan) at 38°C for 35 min. Compounds from our in-house library, which have been described elsewhere[54], were tested at a concentration of 200 µM [corresponding to a final concentration of 1% (v/v) dimethyl sulfoxide (DMSO)] by adding 0.5 µL of a 20 mM solution of compounds to the wells before starting the experiment. The control corresponded to 1% DMSO.

Compound **696** was synthesized, as described in the supporting information (supplementary scheme S1). End-point samples from the *in vitro* assembly assay in the presence of either compound **696** or 1% DMSO (control) were used for the disassembly assay. Briefly, these samples were centrifuged at 20,000 × *g* for 20 min at room temperature and resuspended in 400 µL of low-salinity buffer (50 mM NaCl). Aliquots were sampled immediately after resuspension (t0) and at 8, 24, or 32 h thereafter. Aliquots were centrifuged immediately after sampling at 20,000 × *g* for 20 min at room temperature, and the pellets were collected and analyzed using 12% SDS-PAGE. Gels were stained using Instant*Blue*™ reagent (Expedeon). Gel images were acquired using a Fusion Fx camera (Vilber).

MST. MST experiments were performed, as previously described[54]. Briefly, we measured with a Monolith NT.115 instrument (NanoTemper Technologies) the diffusion of the fluorescent-labeled protein in capillaries when increasing the temperature of 1°C using an infrared light,. The

diffusion properties of the fluorescent protein will be modified when binding **696**, allowing the estimation of the affinity by titration with serial dilutions of the compound. To this purpose, His-tagged proteins were labeled following the supplier's protocol (NanoTemper Technologies) using the Monolith His-Tag RED-tris-NTA Labeling kit (NanoTemper)[55]. The experiments were carried out at 40% MST power and 60% LED power at 37°C. The compound was tested using serial 2× dilutions, resulting in a concentration range between 1 mM and 31 nM. Kd estimation (data points averaging and curve fitting using the Kd model) was automatically calculated from the measured MST traces using the manufacturer's software (MO.Affinity Analysis 3).

Singly labeled ^{15}N protein. *Escherichia coli* bacteria (T7 Express Competent *E. coli* strain, New England Biolabs) were transformed with pRSET-p24EΔCP-T, as previously described[56]. One colony was grown overnight in lysogenic broth (LB) media at 37°C. The inoculation was performed using 20 mL of this preculture per L of culture. The LB preculture volume used for inoculation was centrifuged for 5 min at 6,000 × *g* at room temperature to pellet the bacteria, the LB supernatant was removed, and bacteria were resuspended in M9 minimum media containing 4 g/L glucose, 1× MEM vitamins, 1 mM $MgSO_4$, 100 µM $CaCl_2$, 6 g/L Na_2HPO_4, 3 g/L KH_2PO_4, 5 g/L NaCl, 0.5 g/L ISOGRO-^{15}N Powder-Growth medium (all supplied by Sigma-Aldrich), and 1 g/L $^{15}NH_4Cl$ (Euriso Top). Media were supplemented with ampicillin (Sigma-Aldrich) at a final concentration of 50 µg/L. After inoculation, bacteria were grown at 37°C until the OD_{600} reached 0.4; protein expression was induced using 1 mM isopropyl-β-D-thiogalactopyranoside (Sigma-Aldrich). Bacterial cells were then grown overnight at 25°C and centrifuged for 5 min at 6,000 × *g* at room temperature. Pellets were stored at –20°C until use.

Triple-labeled ^{15}N, ^{13}C, D protein. Bacteria were grown as described above for singly labeled protein but in M9 media prepared using D_2O (Sigma-Aldrich), deuterated ISOGRO-^{13}C,^{15}N, D

(Sigma-Aldrich), and 2 g/L D-glucose-$^{13}C_6$,1,2,3,4,5,6,6-d_7 (Euriso Top). Preculture and culture were performed, as described above, with inoculation in M9 media until the preculture reached a final OD_{600} of 0.1.

Bacterial lysis. Bacteria were lysed by sonication (40% power, 2-min cycles) on ice at least three times until the medium was not viscous. Cell debris was then pelleted using centrifugation for 20 min at 11,000 × *g* at 4°C, and supernatants were purified using affinity chromatography.

Protein purification. We performed affinity chromatography for 6×His-tagged proteins using the Ni-TED resin (Macherey-Nagel) and removed the His tag using Factor Xa, as previously described[56]. The protein was then concentrated using a Vivaspin 20 centrifugal concentrator (10,000 MWCO; polyethersulfone, Sartorius Stedim Lab Ltd.) and stored in 50 mM phosphate buffer (pH 6.8) containing 50 mM NaCl and 2 mM DTT. Protein concentration was assessed using a Nanodrop instrument (Thermo Fisher Scientific). The protein solution was supplemented with D_2O at a final concentration of 5%. We used samples at a final concentration of 2.8 mg/mL (120 µM) for the triple-labeled protein for NMR assignment and 2.2 mg/mL (92 µM) for CSP analysis.

NMR acquisition and data processing. A 300-µL aliquot of labeled p24 sample (120 µM) was placed in 5-mm Shigemi tubes. All NMR spectra were recorded at 293 K using an AvanceNeo Bruker 900 MHz spectrometer equipped with a CPTCI cryoprobe. The sequence-specific backbone assignment was based on two-dimensional (2D) TROSY ^1H-^{15}N, and three-dimensional (3D) BEST-TROSY HNCO, BEST-TROSY-HN(CA)CO, BEST-TROSY-HNCACB, BEST-TROSY-HN(CO)CACB, BEST-TROSY-HNCA, BEST-TROSY-HNCOCA, and TROSY-HNCANNH pulse sequences. The proton chemical shifts were referenced using the sodium 3-trimethylsillyl-[2,2,3,3-d4]propionate signal at 0 ppm. Data were transformed and processed using

NMRPipe[57] and qMDD for acquisition with nonuniform sampling[58] and analyzed using CCPN Analysis Suite software[59].

For the determination of CSPs, we used ^{15}N-labeled protein samples (2.2 mg/mL, 90 µM). We acquired HSQC spectra with samples containing compound **696** at a final concentration of 200 µM. Briefly, we added the required volume of compound stock solution diluted in deuterated-DMSO (DMSO-d6), or DMSO-d6 alone as a control, representing 3.3 µL in a protein sample of 330 µL (1% DMSO final).

Combined ^{1}H,^{15}N CSPs were calculated for each peak using the following formula: $CSP = \sqrt{(\delta^1 H)^2 + \frac{\omega_N}{\omega_H}(\delta^{15} N)^2}$ with $\delta^1 H$ and $\delta^{15} N$ as the chemical shift displacements with and without the tested compounds, respectively, and ω_H and ω_N as the spectral widths of ^{1}H and ^{15}N, respectively, yielding $CSP = \sqrt{(\delta^1 H)^2 + 0.237\ (\delta^{15} N)^2}$.

Molecular docking and visualization. We used Chimera software (UCSF) to render the molecular structures[60], while molecular surfaces were plotted using the MSMS tool of the software[61].

The monomeric crystal structure of full-length p24 (PDB entry 5NA2[56]) was used as the target in the docking experiment. Compound **696** was modeled in 3D using its smiles code produced by the ChemDraw software (PerkinElmer Informatics). Both p24 and **696** were then prepared using AutoDockTools (v1.5.6)[62]: The polar hydrogen atoms were added, the nonpolar hydrogens were merged, and the Gasteiger partial atomic charges were computed.

Docking was carried out using the AutoDock Vina (v1.1.2) program[63]. Compound **696** was treated as fully flexible, while the target protein p24 was treated as rigid, with the exception of some residue side chains that were selected in an extended perimeter around the surface binding

site identified by NMR—namely Leu 30, Phe 39, Thr 49, Met 51, Ile 55, Met 56, Cys 61, Asp 64, Lys 65, Glu 66, Ile 67, Leu 68, Asp 69, Glu 70, Leu 72, Lys 73, Thr 76, Asp 80, Met 100, Ile 102, Cys 121, Tyr 125, and Leu 129. The docking grid box was positioned to cover this area, and a large exhaustiveness value of 500 was used to maximize the thoroughness of the search. A visual examination of the best docking poses was performed using PyMOL (Schrödinger, LLC).

We finally used the LigPlot+ program (v2.2)[64] to determine the residues involved in the predicted protein-compound complex and the nature of the interactions (i.e., hydrogen bonds and unbound contacts).

Results

Screening and identification of a specific compound interfering with FIV capsid assembly *in vitro*. The screening of 400 compounds from our in-house chemical library using a spectrophotometric *in vitro* assembly assay[54,65] identified a compound, **696**, belonging to the chemical series of benzimidazole compounds, which delayed capsid assembly (Figure 1).

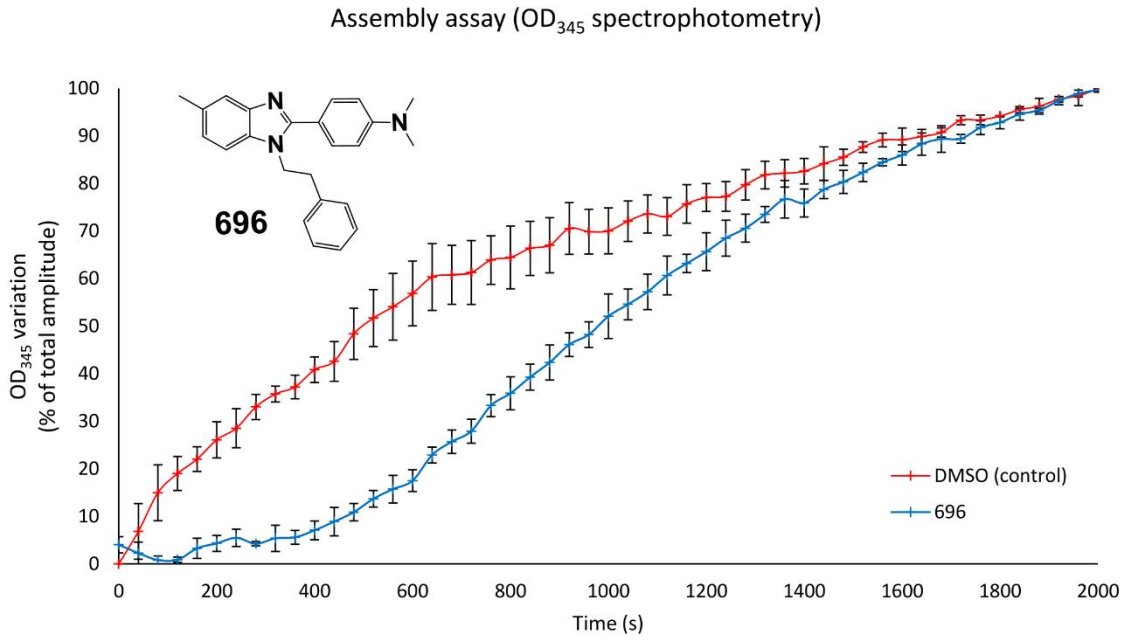

Figure 1. FIV p24 assembly in the absence or presence of compound **696**. The chemical structure of **696** is shown at the top left corner of the graph. Each curve displays the mean of three experiments, with error bars representing standard deviations.

Hence, this compound interferes with capsid assembly. To confirm the specificity of the interaction, MST experiments were performed by titrating serial dilutions of **696** against 200 nM of fluorescent-labeled FIV p24. These experiments revealed an estimated affinity of the lead compound **696** for p24 of 101 µM ± 35 µM (Figure 2).

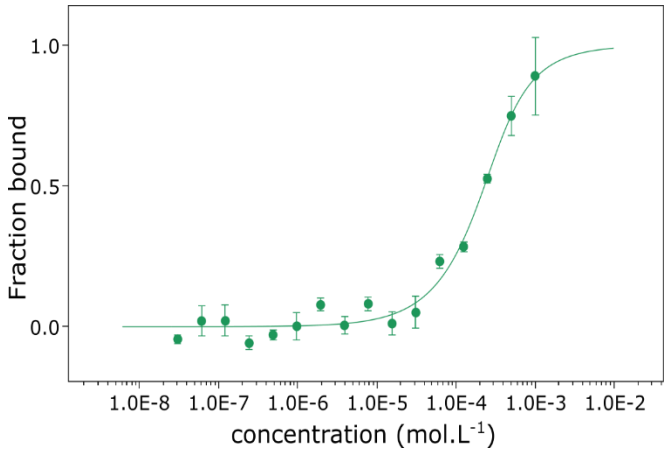

Figure 2. Affinity of p24 for **696** measured by MST. Data points represent the mean of three experiments with error bars corresponding to standard deviations. The curve was plotted automatically using analysis software.

NMR assignment of FIV p24. Since the direct binding of **696** was confirmed by MST, we focused on the identification of its binding site on p24. To this end, we used liquid-state NMR spectroscopy. We used the truncated protein p24EΔCP-T for which the structure was previously determined using X-ray crystallography[56]. The p24 concentration was maintained at 2.8 mg/mL (120 µM) to avoid dimerization or oligomerization of the protein[29] during the NMR

acquisition experiments. Using a ^{15}N,^{13}C,D-triple-labeled FIV p24 sample, we obtained a good-quality 2D ^{1}H,^{15}N-HSQC spectrum using a 900-MHz NMR spectrometer (Figure 3).

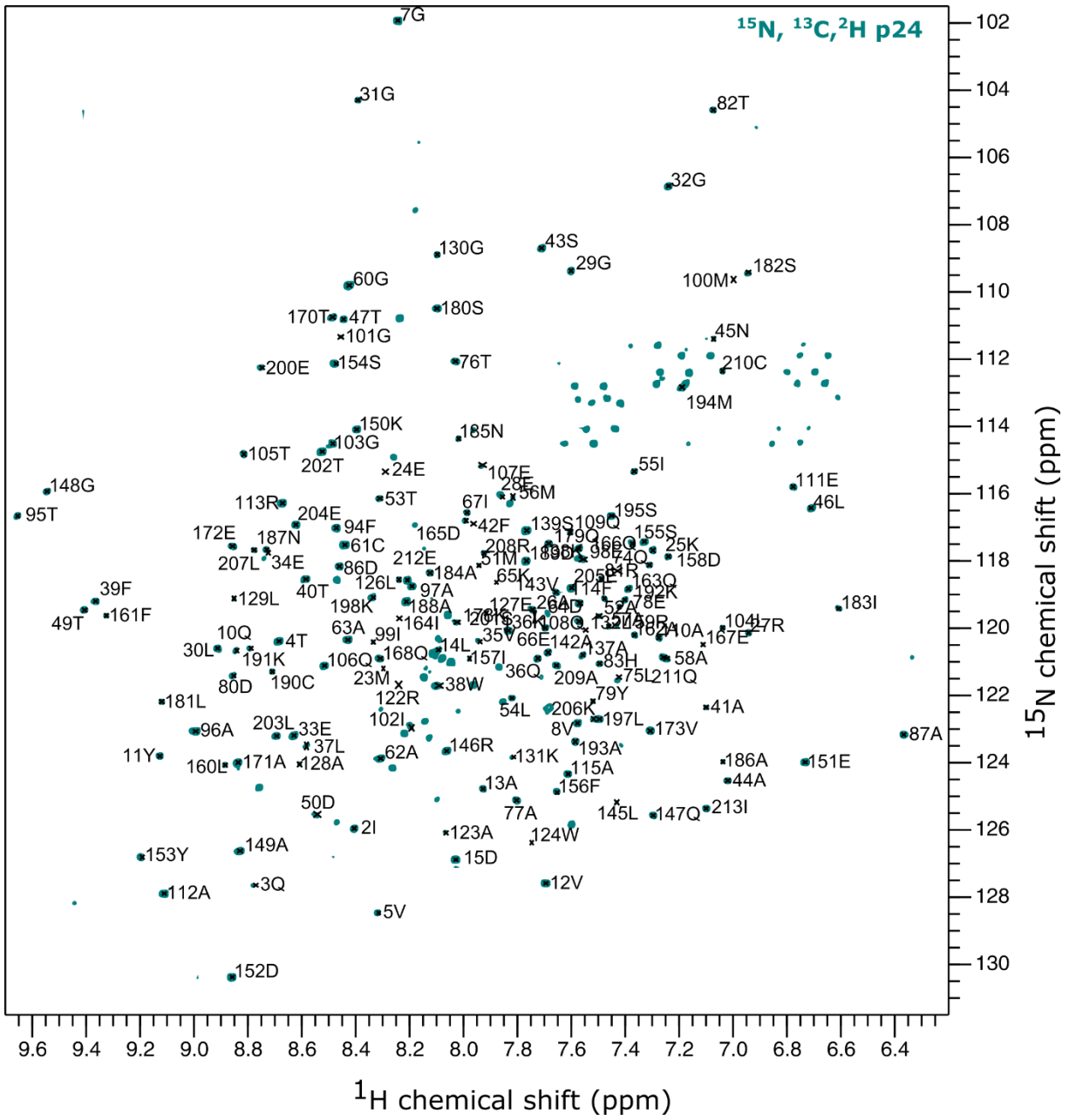

Figure 3. The ^{1}H,^{15}N-HSQC NMR spectrum of FIV p24. The NMR assignment was performed as described in the methods.

As no NMR data were available in the literature for FIV p24, we had to perform the NMR assignment. Thus, we collected the complete NMR dataset on $^{15}N,^{13}C$,D-triple-labeled FIV p24 samples from 3D $^{1}H,^{15}N,^{13}C$-HNCO, HN(CA)CO, HNCA, HN(CO)CA, HNCACB, HN(CO)CACB, and HN(CA)NNH spectra during the sequential assignment process, which was performed using the CcpNmr software[59] (supplementary figure S1).

The NMR assignment of FIV p24 (Figure 3) was deposited in the *Biological Magnetic Resonance Data Bank* (entry **50794**). This assignment covers 167 of the 201 non-proline residues (83% coverage) from the p24 sequence (Figure 4A and B). The missing assignments correspond to regions of the protein for which the signal:noise ratio was of low quality, including residues located in a proline-rich loop (residues Pro 84 to Phe 94) as well as part of helices α4 and α7 (Figure 4C). Using the experimental ^{13}C NMR chemical shifts, we characterized the secondary structure of p24 in solution, which is in complete agreement with the crystal structure[56], thereby confirming the quality of our NMR data (**Figure 4**D).

A)

Category	Type NH	Type HN	Type CO	Type Cα	Type Cβ	All residues
Available	213	200	213	213	204	213
Assigned	167	167	185	185	154	187
% Assigned	78%	84%	87%	87%	75%	88%

B)

```
  1 TIQTVNGVPQYVALDPKMVSIFMEKAREGLGGEEVQLWFTAFSANLTPTD
 51 MATLIMAAPGCAADKEILDESLKQLTAEYDRTHPPDAPRPLPYFTAAEIM
101 GIGLTQEQQAEARFAPARMQCRAWYLEALGKLAAIKAKSPRAVQLRQGAK
151 EDYSSFIDRLFAQIDQEQNTAEVKLYLKQSLSIANANADCKKAMSHLKPE
201 STLEEKLRACQEI
```

C)

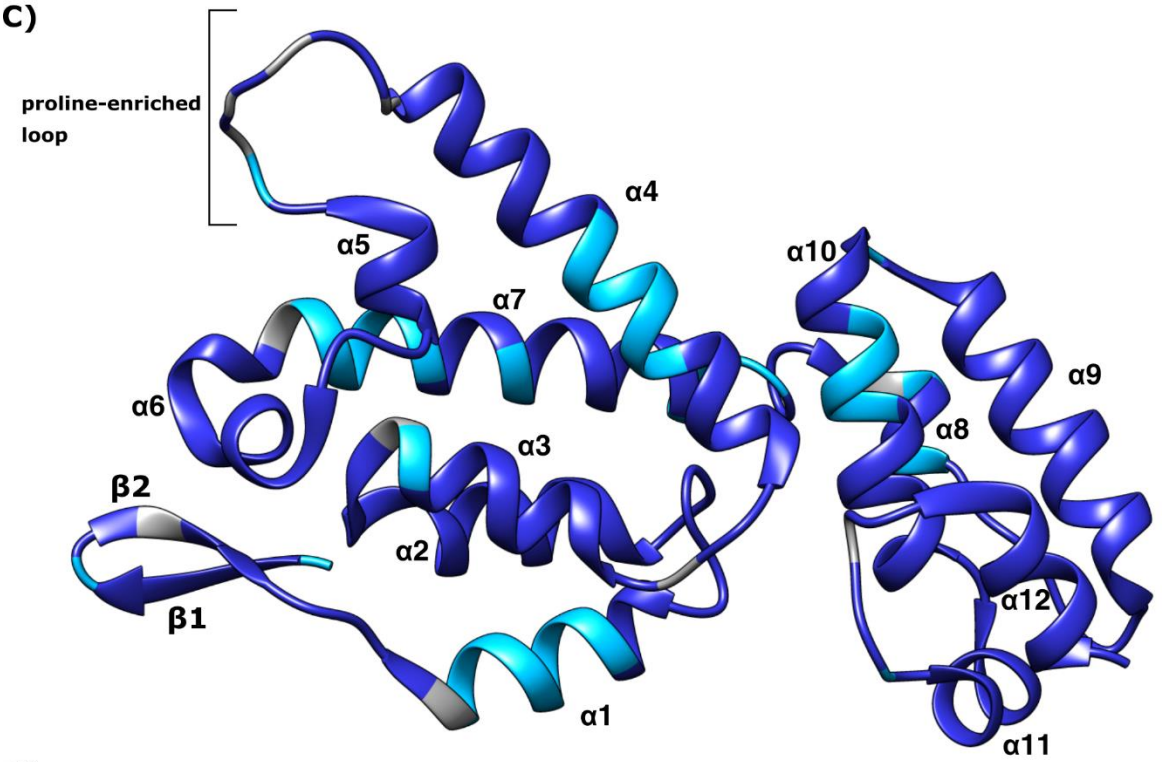

D)

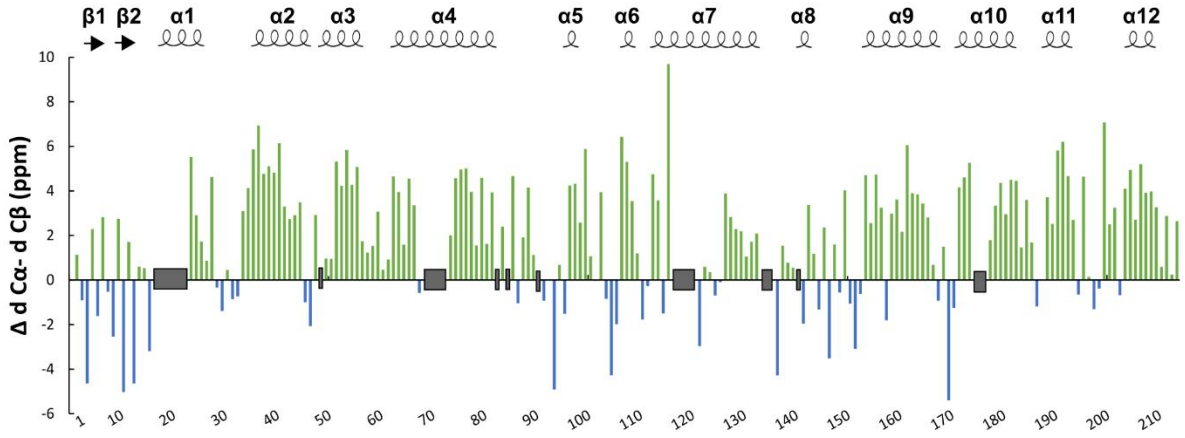

Figure 4. NMR of FIV p24. A) Summary of the p24 NMR signal assignments according to atom type. B) Sequence of p24EΔCP-T. Residues for which the NMR signals were assigned are highlighted in dark blue. C) The p24 structure (PDB entry 5NA2) is colored as follows: assigned amino acids in dark blue, proline residues that do not have a proton amide in grey, and unassigned residues in light blue. Secondary structures are also labeled according to PDB entry 5NA2[56]. D) ^{13}C secondary NMR chemical shifts (dC_α-dC_β) along the p24 sequence, with dC_α and dC_β corresponding to differences between the experimental and random coil chemical shift values for $^{13}C_\alpha$ and $^{13}C_\beta$, respectively. Positive and negative values indicate the presence of an α-helix and a β-strand, respectively. Unassigned residues are displayed as grey boxes. Above the graph are plotted the secondary structures observed for the crystalline structure of FIV p24 (PDB 5NA2[56]).

CSP analysis upon the binding of compound 696. To identify the binding site for the compound in p24, we performed an NMR CSP analysis. For this purpose, we compared the ^{1}H,^{15}N-HSQC spectra of ^{15}N-p24 samples in the absence (control with 1% DMSO-d6) and presence of compound **696** (200 μM, representing the final concentration of 1% DMSO-d6) and calculated the combined ^{1}H and ^{15}N CSPs induced upon binding of the compound (Figure 5). CSPs were observed for a limited set of resonances in which most of the peaks were unaffected; these findings were compatible with a well-defined binding site in p24 (Figure 5).

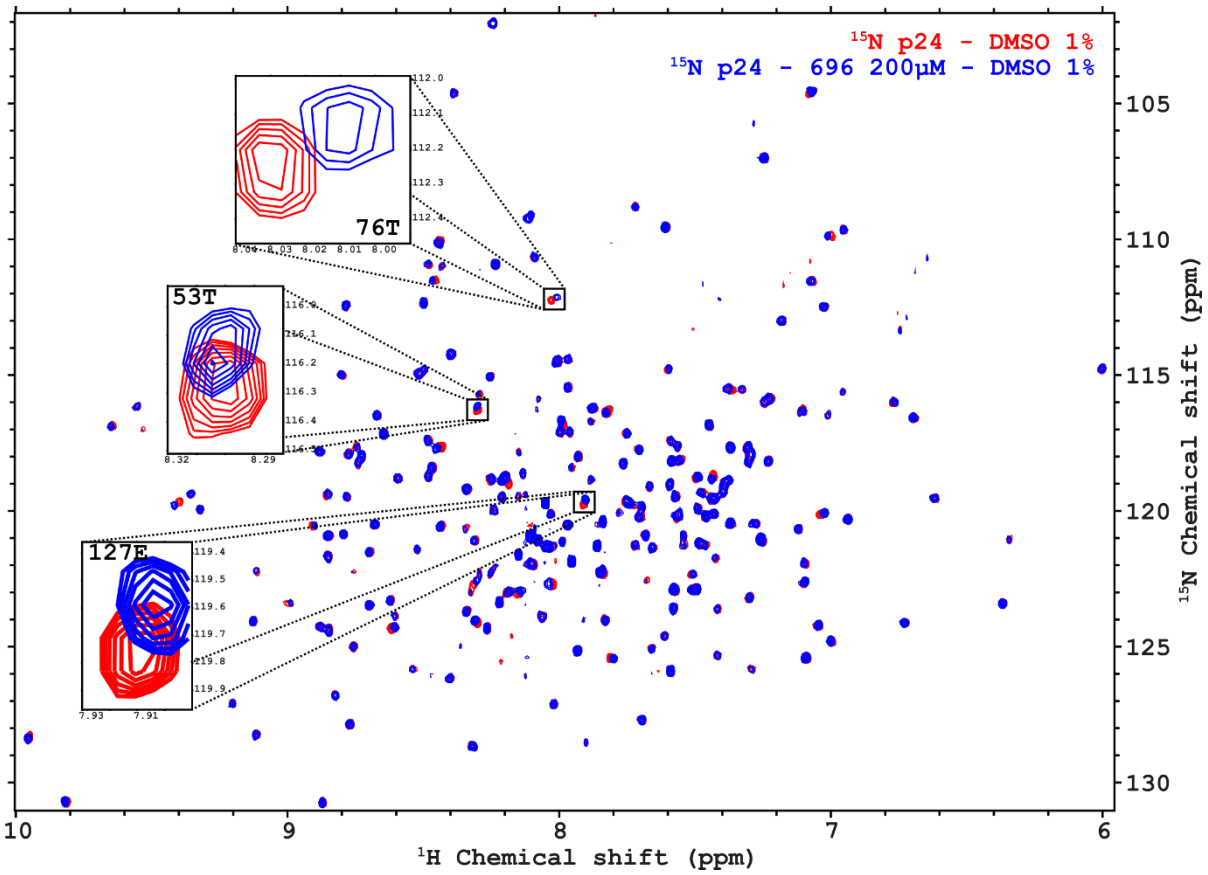

Figure 5. ^{1}H,^{15}N-HSQC NMR spectra of FIV p24. Overlay of 2D spectra of FIV p24 acquired in the absence (red) and presence (blue) of **696** (200 µM). The three resonances with the highest CSPs are enlarged.

After quantification of the ^{1}H and ^{15}N combined CSPs upon binding of compound **696** at 200 µM, 21 resonances in the ^{1}H,^{15}N-HSQC spectrum, corresponding to 21 p24 residues, displayed a CSP higher than a 2× standard deviation (SD), including 11 peaks with CSPs greater than 3× SD. Nine amino acids residues with the highest CSPs colocalized in a define area in the N-terminal domain (**Figure 6**A and B), which were mainly located in helices α3, α4, and α7 (**Figure 6**B). These amino acids define the binding site on the surface of the N-terminal domain of p24 (**Figure 6**C).

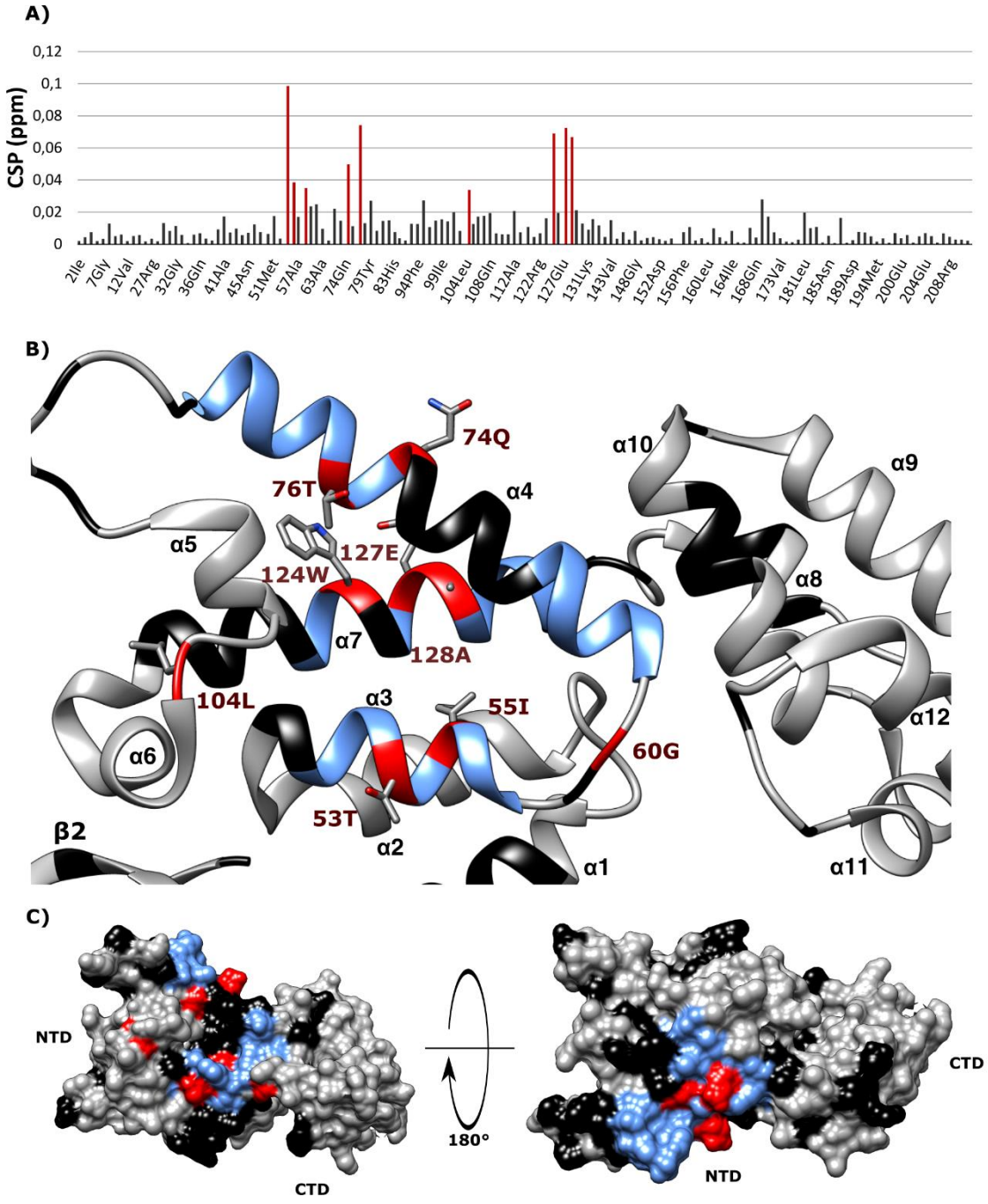

Figure 6. Interaction between p24 and **696**. A) Combined $^{1}H,^{15}N$-NMR CSPs induced in p24 upon **696** binding. The nine residues with the strongest CSPs (>3× SD) are highlighted in red. B) Localization of these nine amino acids (red) in the p24 structure (PDB entry 5NA2 [56]). Helices α3, α4, and α7 are displayed in blue. Amino acids in black are unassigned. C) Mapping of these amino acids on the surface of p24 on opposite sides.

Residues outside this binding site that display high CSPs, such as Leu 104 and Gly 60, may reflect conformational readjustments of the linkers between these helices.

Molecular modeling of the p24/696 interaction and experimental validation. Using these data, we performed a computer-aided molecular docking experiment to further characterize the binding mode of compound **696** to FIV p24. We used the monomeric structure of p24 (PDB entry 5NA2[56]) as a target. The docking search space was selected to encompass the surface area where we observed the NMR CSPs (Figure 6B and C). The peptide backbone was treated as rigid, while the residues side chains inside the above-mentioned area were treated as flexible. As a result, the best docking pose, with a ΔG binding energy estimated at –8.0 kcal/mol, was positioned in the putative binding site between helices α3 and α4 (Figure 7A). We used the LigPlot+ program[64] to determine the predicted interactions between the p24 protein and compound **696** from this best docking solution. We identified nine amino acids involved in hydrogen bonding or hydrophobic interactions with the compound (Figure 7B).

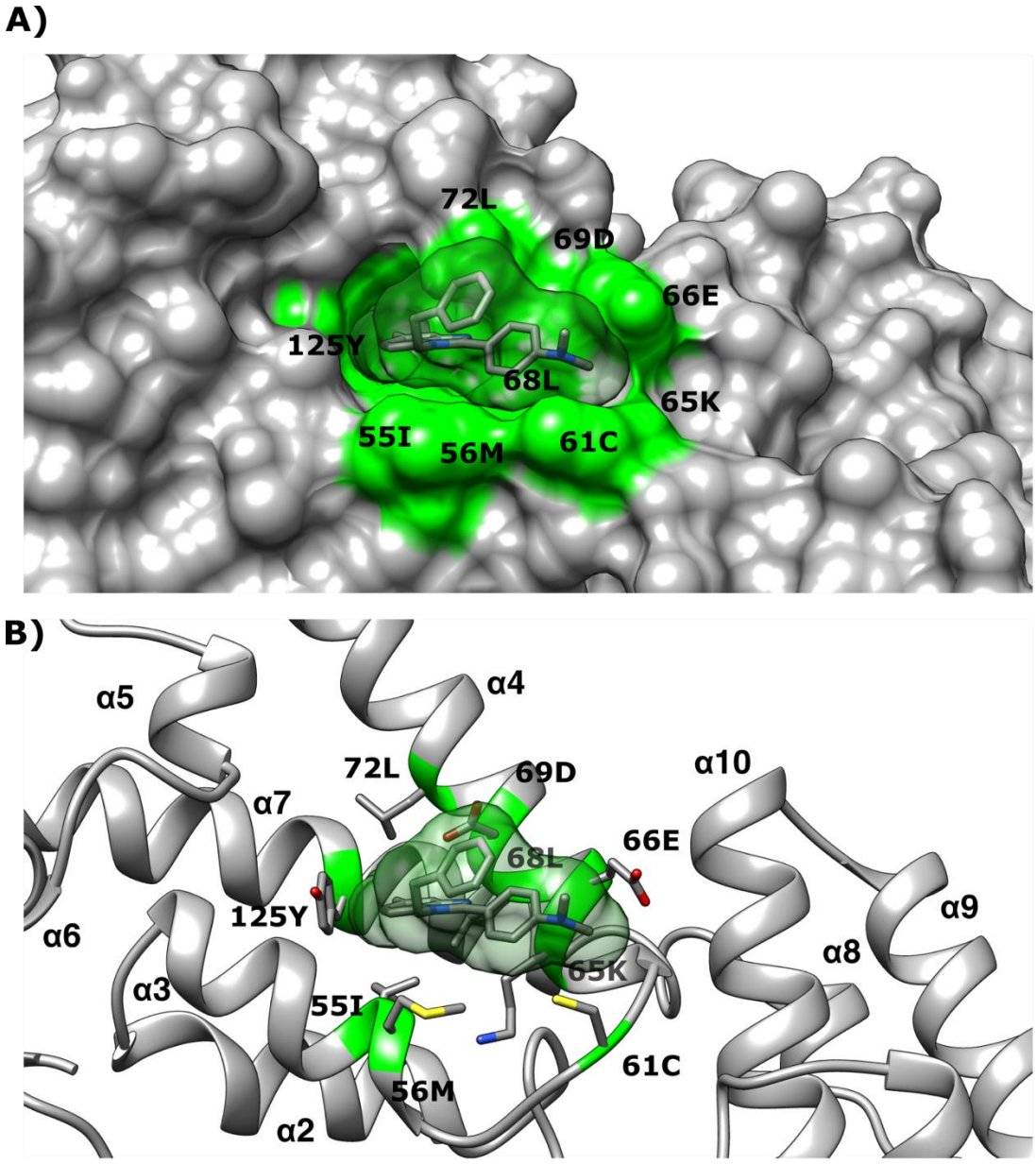

Figure 7. Molecular docking of compound **696** on the p24 surface using experimental NMR data. A) Surface view and B) ribbon view of the best docking solution for **696** (sticks and dark green surface) on p24. The residues identified to be involved in binding by the program LigPlot+ are shown in light green.

We also tested whether compound **696** could interfere with FIV p24 disassembly because this binding region corresponds, in HIV-1 p24, to a zone targeted by antiviral compounds that have been described to stabilize HIV-1 hexamers (e.g., PF74[51]). Assembly products, obtained in the presence or absence of **696** at the end of our assembly experiments (Figure 1), were collected, centrifuged, and resuspended in a low-salinity buffer to promote disassembly. At different time points following the initiation of disassembly (t), samples were centrifuged, and the pellets were analyzed using SDS-PAGE (Figure 8).

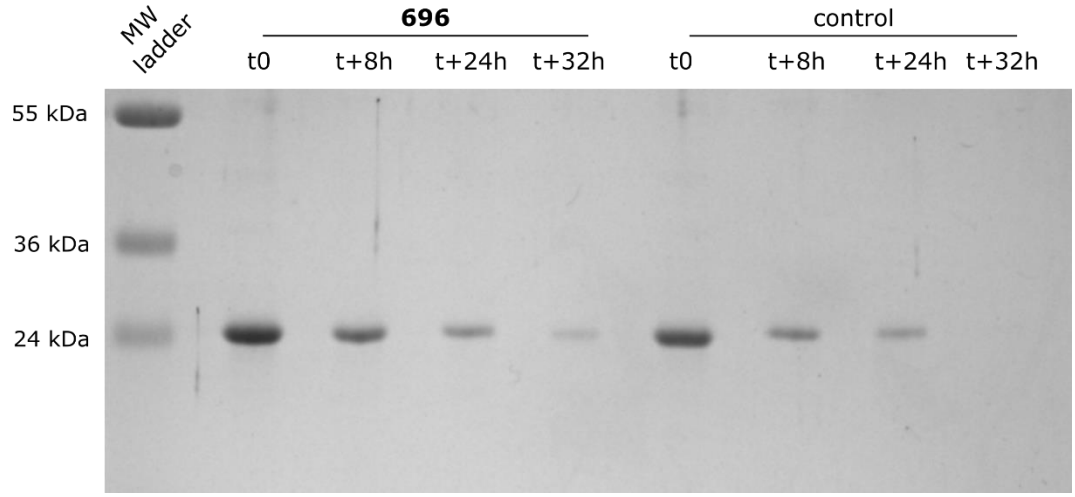

Figure 8. Effect of compound **696** on p24 disassembly analyzed by SDS-PAGE. The assembly of p24 was performed in the presence of either compound **696** or DMSO (control), and the kinetics of disassembly in a low-salinity buffer were then analyzed at several time points (immediately after, and 8, 24, or 32 h after the initiation of disassembly) by SDS-PAGE.

At t + 32 h, assembled p24 was still present in the presence of **696** but not in the untreated control, demonstrating the stabilizing role of **696** during p24 disassembly and re-enforcing our structural identification of the binding site of **696** by NMR and docking experiments.

Discussion

In this study, we identified one promising lead compound, named **696**, which was shown to interfere with FIV capsid assembly/disassembly *in vitro*. The binding of this compound to FIV p24 was confirmed by both MST and NMR spectroscopy. The specific **696**-binding site on p24, involving the α3, α4, and α7 helices, was identified by NMR experiments and refined using molecular modeling.

This paper presents the first NMR assignment for the FIV p24 protein, which covers 83% of the total sequence (BRMB entry **50794**). As observed on the NMR spectra, the quality of the signal is not uniform over the entire protein (supplementary figure S1). The requirement for perdeuteration, as well as disparities in the quality of the NMR signal, remain puzzling, considering the size of the protein (24 kDa), as larger proteins have been assigned previously without perdeuteration[66,67]. Indeed, initially acquired NMR spectra of p24 without perdeuteration showed a poor signal:noise ratio (spectra not shown). In addition, even though the deuterium labeling improved the overall signal:noise ratio, some resonances were still too broad with a very low signal:noise ratio. These observations may be linked to potential low-affinity p24/p24 interactions in the NMR samples, although the protein concentration was maintained at 120 µM to avoid multimerization[29]. HIV-1 p24 subunits of the hexamer were shown to interact with each other through their N-terminal α1, α2, and α3 helices and their C-terminal α9 and α10 helices (PDB entries **3H47** and **3MGE**, respectively)[26]. Moreover, we cannot exclude that certain p24 residues exhibit conformational dynamics on the µs-to-ms scale (intermediate exchange) that could result in line broadening. Although this assignment was incomplete, it was sufficient to identify the **696**-binding site on FIV p24. As no known reference compound targeting FIV p24 has been described to date, our results represent a valuable tool for further studies of ligand-binding sites on FIV p24.

Interestingly, the relatively small number of NMR peaks that underwent CSPs upon **696** binding reveals the existence of a well-defined specific binding site on p24. Based on our NMR assignment, we were able to identify the p24 amino acid residues involved in binding. The combination of NMR spectroscopy and molecular docking allowed us to obtain a structural model of **696** bound to FIV p24. The results are consistent with a binding pocket delimited by the α3, α4, and α7 helices on the protein. We also observed that two residues located outside of the pocket, Gly 60 and Leu 104, underwent CSPs upon inhibitor binding, suggesting a slight conformational readjustment of the loops linking these helices. Because of the ability of p24 to undergo rearrangement during viral assembly and maturation, it is possible that these conformational changes after **696** binding could lead to the decrease in p24 assembly that we observed *in vitro*.

Compound **696** belongs to the benzimidazole family, one of the most common small molecule drug families listed by the U.S. Food and Drug Administration[68]. Some benzimidazoles have already been tested against HIV-1 p24. One (BM2) was shown to bind HIV-1 p24 but at a site delimited by the α1, α2, α3, and α4 helices[69]. These differences in binding sites can be explained by the low sequence homology (29%) between the HIV-1 and FIV p24 proteins[56], which can impact the interactions between the compounds and proteins, or by differences between the chemical groups present on the benzimidazole rings of BM2 and **696**. Nonetheless, interactions between **696** and HIV-1 p24 are currently being tested.

Interestingly, the **696** capsid pocket is structurally conserved in HIV-1, where it is targeted by inhibitors such as PF74 or one of its derivatives, GS-6207, which is currently in clinical trials against HIV[41,49]. These compounds do not inhibit FIV replication *in vitro*[53], but the molecular docking of **696** demonstrates that it interacts with FIV p24 similar to the interaction of PF74 with

HIV-1 p24. It is interesting to note that these HIV-1 inhibitors have been demonstrated to target the p24:p24 interfaces in HIV-1 p24 capsomers[41,49,52].

In HIV-1 p24, the conserved pocket also binds cellular partners such as human Nup153 (Figure 9A, PDB entry **4U0C**) and CPSF6 (data not shown, PDB entry **4U0A**[70]).

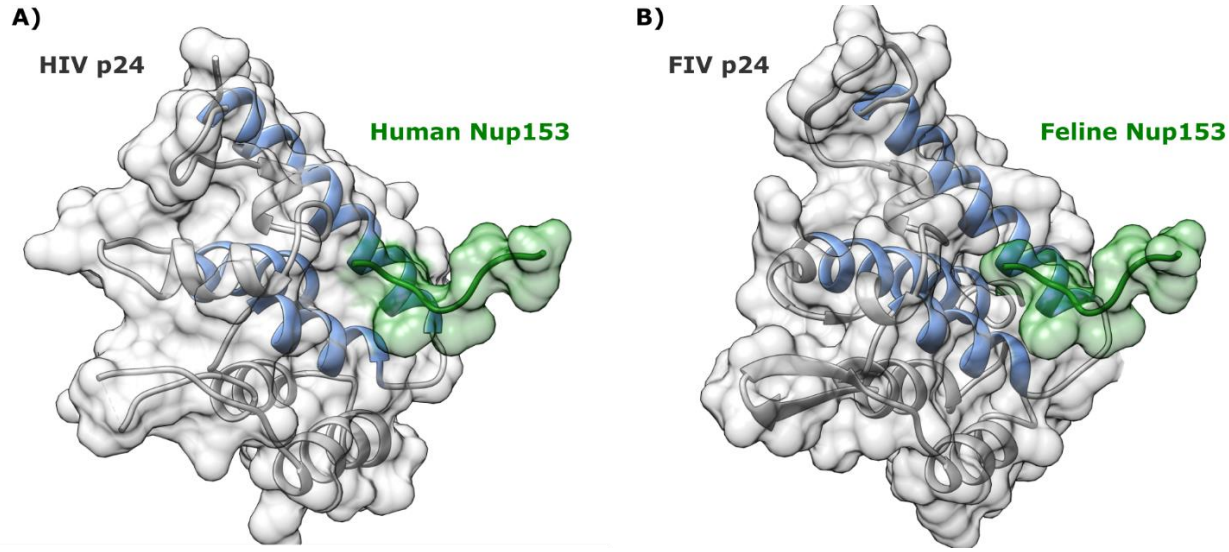

Figure 9. P24/Nup153 interactions. A) The experimental structure of the human Nup153 peptide bound to HIV-1 p24 (PDB entry 4U0C). B) Three-dimensional homology modeling of the feline Nup153 peptide on FIV p24. The α3, α4, and α7 helices are highlighted in blue.

Interestingly, the peptide fragment of human CPSF6, which is implicated in the binding of HIV-1 p24 in the crystal structure, is 100% identical to its counterpart in the feline CPSF6 protein (*Felis catus* sequence: UniProtKB **A0A2I2UG80**, residues 313–327). Both feline Nup153 (fNup153, UniProtKB **M3WFC8**) and human Nup153 have a high sequence identity of 89% for the region of hNup153 identified as interacting with HIV-1 p24. Therefore, we were able to model the binding of feline Nup153 on FIV p24 from the structure of human Nup153–HIV-1 p24 (**Figure 9**B).

We are currently investigating the molecular basis of the interactions between FIV p24 and feline Nup153 and CPSF6 to confirm this hypothesis. Anyhow, these structural similarities between

HIV-1 and FIV p24 and the sequence conservation between human and feline Nup153 and CPSF6 suggest a conserved mechanism of interaction among lentiviruses with cellular partners, as previously described for CypA[38]. We are currently seeking to solve the structure of the FIV p24 hexamer, which would confirm whether **696** indeed interacts with two adjacent monomers of capsomers. Such a finding would allow for structure-based improvements in compound **696** to target both sides of the p24:p24 interface in the hexamers. These observations are highly promising for the rational design of derivatives from **696** targeting FIV p24 that possess potent anti-FIV effects.

The affinity of **696** for monomeric p24 was estimated around 100 µM using MST, which is sufficient to consider **696** a promising lead scaffold for further optimization. Moreover, if **696** behaves in a similar fashion to PF74 and its derivatives[41,49,52] and indeed interacts with two adjacent monomers of FIV p24, the K_d value we obtained using monomeric FIV p24 might be underestimated compared to what it would be using FIV p24 hexamers. Moreover, the low solubility of **696** in water and the requirement for DMSO for its resuspension limit the end-point concentrations we could use in MST or NMR experiments. Consequently, we cannot exclude that the saturating values observed by MST are biased and that the real K_d value is lower than 100 µM. Solubility issues at high concentrations could also explain why the NMR CSP experiments did not reveal additional CSPs at 400 µM (data not shown). Efforts to develop **696**-derived compounds that are more soluble in aqueous buffers will help clarify this point.

Indeed, as **696** is now identified as the first compound to target FIV capsid assembly, derivatives of this reference molecule will be developed based on our NMR and molecular docking data and, when available, the structure of FIV p24 hexamers. These optimized compounds will first be characterized and selected using the strategy described here, and the more promising compounds

will then be tested for their ability to inhibit FIV replication *in cellulo*. As the **696** compound is inexpensive to produce and thus compatible with the needs of veterinary medicine, this optimization strategy could eventually lead to the identification of drugs with better affinities for p24, low costs of synthesis, and antiviral efficacies, thus enabling their widespread use in veterinary practice.

Finally, it should be noted that the NMR assignment and molecular docking protocols we developed, and which were used to characterize the interaction between **696** and FIV p24, may not only be used to assess future **696** derivatives but can more generally be used to rationally design other inhibitory molecules targeting other regions of FIV p24, as described for HIV-1[71]. Taken together, our work represents the first steps towards the development of potent, low-cost inhibitors targeting the FIV p24 protein as a treatment for FIV infection.

Associated content

Accession codes:

- HIV-1 Gag: UniprotKB P04591
- FIV Gag: UniprotKB P16087; subunit p24: BRMB 50794
- Human CypA: UniprotKB P62937
- hNup153: UniprotKB P49790
- hNup358: UniprotKB P49792
- hCPSF6: UniprotKB Q16630
- fCPSF6: UniprotKB A0A2I2UG80
- fNup153: UniprotKB M3WFC8

Author information

Corresponding authors

* Christophe Guillon, Retroviruses and Structural Biochemistry, UMR 5086 - Molecular Microbiology and Structural Biochemistry, CNRS/Université Lyon 1, 7 passage du Vercors, 69367 Lyon cedex 07, France. Phone: +33 437652904. E-mail: christophe.guillon@ibcp.fr

* Guzmán Alvarez: Laboratorio de Moléculas Bioactivas, Centro Universitario Regional Litoral Norte, Universidad de la República, Estación Experimental "Dr. Mario A. Cassinoni", Ruta 3 km 363, 60000 Paysandú, Uruguay. Phone: +598 47227950. E-mail: guzmanalvarezlqo@gmail.com

Author contributions

C.G. and G.A designed and coordinated the experiments. M.L. performed protein expression and purification. M.L and C.G performed MST experiments. N.S. performed compounds synthesis and capsid assembly assays. F.-X.C., E.B. and X.H. acquired the NMR spectra. F.-X.C., E.B., X.H. and M.L. interpreted the NMR data and attributed the amino acids. X.R. performed the molecular docking. M.L, X.H, X.R, G.A, P.G and C.G analyzed the data. All authors contributed to the writing of the paper.

Funding sources

This work was supported by ECOS-Sud program U14S01 (Uruguay-France), French Ministry of Research, and by CSIC (Comisión Sectorial de Investigación Científica) program iniciación a la investigación 2017 number ID275. Financial support from the IR-RMN-THC Fr3050 CNRS for conducting the research is gratefully acknowledged.

Notes

The authors declare no conflicts of interest.

Acknowledgments

We thank M. Dujardin and L. Lecoq for their advices in NMR, and R. Monserret and C. Freton for their help with MST. Molecular graphics and analyses performed with UCSF Chimera, developed by the Resource for

Biocomputing, Visualization, and Informatics at the University of California, San Francisco, with support from NIH P41-GM103311.

Supporting Information

Supporting information content:

Figure S1. Examples of NMR strips of HN(CO)CACB and HNCACB experiments used for sequential assignment (residues 206-213).

Scheme S1. Synthetic steps for the preparation of **696** and**,** detailed Methods for the synthesis of **696**

References

(1) Pedersen, N. C., Ho, E. W., Brown, M. L., Yamamoto, J. K. (1987) Isolation of a T-Lymphotropic Virus from Domestic Cats with an Immunodeficiency-like Syndrome. *Science 235*, 790–793.

(2) Brown, M. A., Munkhtsog, B., Troyer, J. L., Ross, S., Sellers, R., Fine, A. E., Swanson, W. F., Roelke, M. E., O'Brien, S. J. (2010) Feline Immunodeficiency Virus (FIV) in Wild Pallas' Cats. *Vet. Immunol. Immunopathol. 134*, 90–95.

(3) O'Brien, S. J., Troyer, J. L., Brown, M. A., Johnson, W. E., Antunes, A., Roelke, M. E., Pecon-Slattery, J. (2012) Emerging Viruses in the Felidae: Shifting Paradigms. *Viruses 4*, 236–257.

(4) Roelke, M. E., Brown, M. A., Troyer, J. L., Winterbach, H., Winterbach, C., Hemson, G., Smith, D., Johnson, R. C., Pecon-Slattery, J., Roca, A. L., Alexander, K. A., Klein, L., Martelli,

P., Krishnasamy, K., O'Brien, S. J. (2009) Pathological Manifestations of Feline Immunodeficiency Virus (FIV) Infection in Wild African Lions. *Virology 390*, 1–12.

(5) Mohammadi, H., Bienzle, D. (2012) Pharmacological Inhibition of Feline Immunodeficiency Virus (FIV). *Viruses 4*, 708–724.

(6) Mora, M., Napolitano, C., Ortega, R., Poulin, E., Pizarro-Lucero, J. (2015) Feline Immunodeficiency Virus and Feline Leukemia Virus Infection in Free-Ranging Guignas (Leopardus Guigna) and Sympatric Domestic Cats in Human Perturbed Landscapes on Chiloé Island, Chile. *J. Wildl. Dis. 51*, 199–208.

(7) Sahay, B., Yamamoto, J. K. (2018) Lessons Learned in Developing a Commercial FIV Vaccine: The Immunity Required for an Effective HIV-1 Vaccine. *Viruses 10*, 277.

(8) Hosie, M. J., Techakriengkrai, N., Bęczkowski, P. M., Harris, M., Logan, N., Willett, B. J. (2017) The Comparative Value of Feline Virology Research: Can Findings from the Feline Lentiviral Vaccine Be Translated to Humans? *Vet. Sci. 4*, 7.

(9) Miller, C., Emanuelli, M., Fink, E., Musselman, E., Mackie, R., Troyer, R., Elder, J., VandeWoude, S. (2018) FIV Vaccine with Receptor Epitopes Results in Neutralizing Antibodies but Does Not Confer Resistance to Challenge. *Npj Vaccines 3*, 1–12.

(10) Troyer, J. L., Pecon-Slattery, J., Roelke, M. E., Johnson, W., VandeWoude, S., Vazquez-Salat, N., Brown, M., Frank, L., Woodroffe, R., Winterbach, C., Winterbach, H., Hemson, G., Bush, M., Alexander, K. A., Revilla, E., O'Brien, S. J. (2005) Seroprevalence and Genomic Divergence of Circulating Strains of Feline Immunodeficiency Virus among Felidae and Hyaenidae Species. *J. Virol. 79*, 8282–8294.

(11) Bendinelli, M., Pistello, M., Lombardi, S., Poli, A., Garzelli, C., Matteucci, D., Ceccherini-Nelli, L., Malvaldi, G., Tozzini, F. (1995) Feline Immunodeficiency Virus: An Interesting Model for AIDS Studies and an Important Cat Pathogen. *Clin. Microbiol. Rev. 8*, 87–112.

(12) Elder, J. H., Lin, Y.-C., Fink, E., Grant, C. K. (2010) Feline Immunodeficiency Virus (FIV) as a Model for Study of Lentivirus Infections: Parallels with HIV. *Curr. HIV Res. 8*, 73–80.

(13) Meeker, R. B., Hudson, L. (2017) Feline Immunodeficiency Virus Neuropathogenesis: A Model for HIV-Induced CNS Inflammation and Neurodegeneration. *Vet. Sci. 4*, 14.

(14) Yamamoto, J. K., Sanou, M. P., Abbott, J. R., Coleman, J. K. (2010) Feline Immunodeficiency Virus Model for Designing HIV/AIDS Vaccines. *Curr. HIV Res. 8*, 14–25.

(15) Schwartz, A. M., McCrackin, M. A., Schinazi, R. F., Hill, P. B., Vahlenkamp, T. W., Tompkins, M. B., Hartmann, K. (2014) Antiviral Efficacy of Nine Nucleoside Reverse Transcriptase Inhibitors against Feline Immunodeficiency Virus in Feline Peripheral Blood Mononuclear Cells. *Am. J. Vet. Res. 75*, 273–281.

(16) Smyth, N. R., McCracken, C., Gaskell, R. M., Cameron, J. M., Coates, J. A., Gaskell, C. J., Hart, C. A., Bennett, M. (1994) Susceptibility in Cell Culture of Feline Immunodeficiency Virus to Eighteen Antiviral Agents. *J. Antimicrob. Chemother. 34*, 589–594.

(17) Hartmann, K., Wooding, A., Bergmann, M. (2015) Efficacy of Antiviral Drugs against Feline Immunodeficiency Virus. *Vet. Sci. 2*, 456–476.

(18) Abdusetir Cerfoglio, J. C., González, S. A., Affranchino, J. L. (2014) Structural Elements in the Gag Polyprotein of Feline Immunodeficiency Virus Involved in Gag Self-Association and Assembly. *J. Gen. Virol. 95*, 2050–2059.

(19) Affranchino, J. L., González, S. A. (2010) In Vitro Assembly of the Feline Immunodeficiency Virus Gag Polyprotein. *Virus Res. 150*, 153–157.

(20) González, S. A., Affranchino, J. L. (2018) Properties and Functions of Feline Immunodeficiency Virus Gag Domains in Virion Assembly and Budding. *Viruses 10*, 261.

(21) Nath, M. D., Peterson, D. L. (2001) In Vitro Assembly of Feline Immunodeficiency Virus Capsid Protein: Biological Role of Conserved Cysteines. *Arch. Biochem. Biophys. 392*, 287–294.

(22) Ovejero, C. A., González, S. A., Affranchino, J. L. (2019) The Conserved Tyr176/Leu177 Motif in the α-Helix 9 of the Feline Immunodeficiency Virus Capsid Protein Is Critical for Gag Particle Assembly. *Viruses 11*, 816.

(23) Kutluay, S. B., Bieniasz, P. D. (2010) Analysis of the Initiating Events in HIV-1 Particle Assembly and Genome Packaging. *PLoS Pathog. 6*, e1001200.

(24) Ganser, B. K., Li, S., Klishko, V. Y., Finch, J. T., Sundquist, W. I. (1999) Assembly and Analysis of Conical Models for the HIV-1 Core. *Science 283*, 80–83.

(25) Pornillos, O., Ganser-Pornillos, B. K., Yeager, M. (2011) Atomic-Level Modelling of the HIV Capsid. *Nature 469*, 424–427.

(26) Pornillos, O., Ganser-Pornillos, B. K., Kelly, B. N., Hua, Y., Whitby, F. G., Stout, C. D., Sundquist, W. I., Hill, C. P., Yeager, M. (2009) X-Ray Structures of the Hexameric Building Block of the HIV Capsid. *Cell 137*, 1282–1292.

(27) Tomasini, M. D., Johnson, D. S., Mincer, J. S., Simon, S. M. (2018) Modeling the Dynamics and Kinetics of HIV-1 Gag during Viral Assembly. *PLoS ONE 13*, e0196133.

(28) Sundquist, W. I., Kräusslich, H.-G. (2012) HIV-1 Assembly, Budding, and Maturation. *Cold Spring Harb. Perspect. Med. 2*, a006924.

(29) Serrière, J., Fenel, D., Schoehn, G., Gouet, P., Guillon, C. (2013) Biophysical Characterization of the Feline Immunodeficiency Virus P24 Capsid Protein Conformation and In Vitro Capsid Assembly. *PLoS ONE 8*, e56424.

(30) Dharan, A., Bachmann, N., Talley, S., Zwikelmaier, V., Campbell, E. M. (2020) Nuclear Pore Blockade Reveals That HIV-1 Completes Reverse Transcription and Uncoating in the Nucleus. *Nat. Microbiol. 5*, 1088–1095.

(31) Dismuke, D. J., Aiken, C. (2006) Evidence for a Functional Link between Uncoating of the Human Immunodeficiency Virus Type 1 Core and Nuclear Import of the Viral Preintegration Complex. *J. Virol. 80*, 3712–3720.

(32) Jacques, D. A., McEwan, W. A., Hilditch, L., Price, A. J., Towers, G. J., James, L. C. (2016) HIV-1 Uses Dynamic Capsid Pores to Import Nucleotides and Fuel Encapsidated DNA Synthesis. *Nature 536*, 349–353.

(33) Zhou, L., Sokolskaja, E., Jolly, C., James, W., Cowley, S. A., Fassati, A. (2011) Transportin 3 Promotes a Nuclear Maturation Step Required for Efficient HIV-1 Integration. *PLoS Pathog. 7*, e1002194.

(34) Selyutina, A., Persaud, M., Lee, K., KewalRamani, V., Diaz-Griffero, F. (2020) Nuclear Import of the HIV-1 Core Precedes Reverse Transcription and Uncoating. *Cell Rep. 32*, 108201.

(35) Dharan, A., Campbell, E. M. (2018) Role of Microtubules and Microtubule-Associated Proteins in HIV-1 Infection. *J. Virol. 92*, e00085-18.

(36) Fernandez, J., Portilho, D. M., Danckaert, A., Munier, S., Becker, A., Roux, P., Zambo, A., Shorte, S., Jacob, Y., Vidalain, P.-O., Charneau, P., Clavel, F., Arhel, N. J. (2015) Microtubule-Associated Proteins 1 (MAP1) Promote Human Immunodeficiency Virus Type I (HIV-1) Intracytoplasmic Routing to the Nucleus. *J. Biol. Chem. 290*, 4631–4646.

(37) Pawlica, P., Berthoux, L. (2014) Cytoplasmic Dynein Promotes HIV-1 Uncoating. *Viruses 6*, 4195–4211.

(38) Goldstone, D. C., Yap, M. W., Robertson, L. E., Haire, L. F., Taylor, W. R., Katzourakis, A., Stoye, J. P., Taylor, I. A. (2010) Structural and Functional Analysis of Prehistoric Lentiviruses Uncovers an Ancient Molecular Interface. *Cell Host Microbe 8*, 248–259.

(39) Arhel, N. (2010) Revisiting HIV-1 Uncoating. *Retrovirology 7*, 96.

(40) Burdick, R. C., Li, C., Munshi, M., Rawson, J. M. O., Nagashima, K., Hu, W.-S., Pathak, V. K. (2020) HIV-1 Uncoats in the Nucleus near Sites of Integration. *Proc. Natl. Acad. Sci. U. S. A. 117*, 5486–5493.

(41) Bhattacharya, A., Alam, S. L., Fricke, T., Zadrozny, K., Sedzicki, J., Taylor, A. B., Demeler, B., Pornillos, O., Ganser-Pornillos, B. K., Diaz-Griffero, F., Ivanov, D. N., Yeager, M. (2014) Structural Basis of HIV-1 Capsid Recognition by PF74 and CPSF6. *Proc. Natl. Acad. Sci. U. S. A. 111*, 18625–18630.

(42) Xie, L., Chen, L., Zhong, C., Yu, T., Ju, Z., Wang, M., Xiong, H., Zeng, Y., Wang, J., Hu, H., Hou, W., Feng, Y. (2020) MxB Impedes the NUP358-Mediated HIV-1 Pre-Integration Complex Nuclear Import and Viral Replication Cooperatively with CPSF6. *Retrovirology 17*, 16.

(43) Matreyek, K. A., Yücel, S. S., Li, X., Engelman, A. (2013) Nucleoporin NUP153 Phenylalanine-Glycine Motifs Engage a Common Binding Pocket within the HIV-1 Capsid Protein to Mediate Lentiviral Infectivity. *PLoS Pathog. 9*, e1003693.

(44) Price, A. J., Fletcher, A. J., Schaller, T., Elliott, T., Lee, K., KewalRamani, V. N., Chin, J. W., Towers, G. J., James, L. C. (2012) CPSF6 Defines a Conserved Capsid Interface That Modulates HIV-1 Replication. *PLoS Pathog. 8*, e1002896.

(45) Tang, C., Loeliger, E., Kinde, I., Kyere, S., Mayo, K., Barklis, E., Sun, Y., Huang, M., Summers, M. F. (2003) Antiviral Inhibition of the HIV-1 Capsid Protein. *J. Mol. Biol. 327*, 1013–1020.

(46) Kortagere, S., Madani, N., Mankowski, M. K., Schön, A., Zentner, I., Swaminathan, G., Princiotto, A., Anthony, K., Oza, A., Sierra, L.-J., Passic, S. R., Wang, X., Jones, D. M., Stavale, E., Krebs, F. C., Martín-García, J., Freire, E., Ptak, R. G., Sodroski, J., Cocklin, S., Smith, A. B. (2012) Inhibiting Early-Stage Events in HIV-1 Replication by Small-Molecule Targeting of the HIV-1 Capsid. *J. Virol. 86*, 8472–8481.

(47) Zhang, H., Zhao, Q., Bhattacharya, S., Waheed, A. A., Tong, X., Hong, A., Heck, S., Curreli, F., Goger, M., Cowburn, D., Freed, E. O., Debnath, A. K. (2008) A Cell-Penetrating Helical Peptide as a Potential HIV-1 Inhibitor. *J. Mol. Biol. 378*, 565–580.

(48) Sticht, J., Humbert, M., Findlow, S., Bodem, J., Müller, B., Dietrich, U., Werner, J., Kräusslich, H.-G. (2005) A Peptide Inhibitor of HIV-1 Assembly in Vitro. *Nat. Struct. Mol. Biol. 12*, 671–677.

(49) Link, J. O., Rhee, M. S., Tse, W. C., Zheng, J., Somoza, J. R., Rowe, W., Begley, R., Chiu, A., Mulato, A., Hansen, D., Singer, E., Tsai, L. K., Bam, R. A., Chou, C.-H., Canales, E., Brizgys, G., Zhang, J. R., Li, J., Graupe, M., Morganelli, P., Liu, Q., Wu, Q., Halcomb, R. L., Saito, R. D., Schroeder, S. D., Lazerwith, S. E., Bondy, S., Jin, D., Hung, M., Novikov, N., Liu, X., Villaseñor, A. G., Cannizzaro, C. E., Hu, E. Y., Anderson, R. L., Appleby, T. C., Lu, B., Mwangi, J., Liclican, A., Niedziela-Majka, A., Papalia, G. A., Wong, M. H., Leavitt, S. A., Xu, Y., Koditek, D., Stepan, G. J., Yu, H., Pagratis, N., Clancy, S., Ahmadyar, S., Cai, T. Z., Sellers, S., Wolckenhauer, S. A., Ling, J., Callebaut, C., Margot, N., Ram, R. R., Liu, Y.-P., Hyland, R., Sinclair, G. I., Ruane, P. J., Crofoot, G. E., McDonald, C. K., Brainard, D. M., Lad, L., Swaminathan, S., Sundquist, W. I., Sakowicz, R., Chester, A. E., Lee, W. E., Daar, E. S., Yant, S. R., Cihlar, T. (2020) Clinical Targeting of HIV Capsid Protein with a Long-Acting Small Molecule. *Nature 584*, 614–618.

(50) Rihn, S. J., Wilson, S. J., Loman, N. J., Alim, M., Bakker, S. E., Bhella, D., Gifford, R. J., Rixon, F. J., Bieniasz, P. D. (2013) Extreme Genetic Fragility of the HIV-1 Capsid. *PLoS Pathog. 9*, e1003461.

(51) Balasubramaniam, M., Zhou, J., Addai, A., Martinez, P., Pandhare, J., Aiken, C., Dash, C. (2019) PF74 Inhibits HIV-1 Integration by Altering the Composition of the Preintegration Complex. *J. Virol. 93*, e01741-18.

(52) McArthur, C., Gallazzi, F., Quinn, T. P., Singh, K. (2019) HIV Capsid Inhibitors Beyond PF74. *Diseases 7*, 56.

(53) Fricke, T., Buffone, C., Opp, S., Valle-Casuso, J., Diaz-Griffero, F. (2014) BI-2 Destabilizes HIV-1 Cores during Infection and Prevents Binding of CPSF6 to the HIV-1 Capsid. *Retrovirology 11*, 1–7.

(54) Sierra, N., Folio, C., Robert, X., Long, M., Guillon, C., Álvarez, G. (2018) Looking for Novel Capsid Protein Multimerization Inhibitors of Feline Immunodeficiency Virus. *Pharmaceuticals 11*, 67.

(55) Seidel, S. A. I., Dijkman, P. M., Lea, W. A., van den Bogaart, G., Jerabek-Willemsen, M., Lazic, A., Joseph, J. S., Srinivasan, P., Baaske, P., Simeonov, A., Katritch, I., Melo, F. A., Ladbury, J. E., Schreiber, G., Watts, A., Braun, D., Duhr, S. (2013) Microscale Thermophoresis Quantifies Biomolecular Interactions under Previously Challenging Conditions. *Methods 59*, 301–315.

(56) Folio, C., Sierra, N., Dujardin, M., Alvarez, G., Guillon, C. (2017) Crystal Structure of the Full-Length Feline Immunodeficiency Virus Capsid Protein Shows an N-Terminal β-Hairpin in the Absence of N-Terminal Proline. *Viruses 9*, 335.

(57) Delaglio, F., Grzesiek, S., Vuister, G. W., Zhu, G., Pfeifer, J., Bax, A. (1995) NMRPipe: A Multidimensional Spectral Processing System Based on UNIX Pipes. *J. Biomol. NMR 6*, 277–293.

(58) Mayzel, M., Rosenlöw, J., Isaksson, L., Orekhov, V. Y. (2014) Time-Resolved Multidimensional NMR with Non-Uniform Sampling. *J. Biomol. NMR 58*, 129–139.

(59) Vranken, W. F., Boucher, W., Stevens, T. J., Fogh, R. H., Pajon, A., Llinas, M., Ulrich, E. L., Markley, J. L., Ionides, J., Laue, E. D. (2005) The CCPN Data Model for NMR Spectroscopy: Development of a Software Pipeline. *Proteins 59*, 687–696.

(60) Pettersen, E. F., Goddard, T. D., Huang, C. C., Couch, G. S., Greenblatt, D. M., Meng, E. C., Ferrin, T. E. (2004) UCSF Chimera--a Visualization System for Exploratory Research and Analysis. *J. Comput. Chem. 25*, 1605–1612.

(61) Sanner, M. F., Olson, A. J., Spehner, J. C. (1996) Reduced Surface: An Efficient Way to Compute Molecular Surfaces. *Biopolymers 38*, 305–320.

(62) Morris, G. M., Huey, R., Lindstrom, W., Sanner, M. F., Belew, R. K., Goodsell, D. S., Olson, A. J. (2009) AutoDock4 and AutoDockTools4: Automated Docking with Selective Receptor Flexibility. *J. Comput. Chem. 30*, 2785–2791.

(63) Trott, O., Olson, A. J. (2010) AutoDock Vina: Improving the Speed and Accuracy of Docking with a New Scoring Function, Efficient Optimization, and Multithreading. *J. Comput. Chem. 31*, 455–461.

(64) Laskowski, R. A., Swindells, M. B. (2011) LigPlot+: Multiple Ligand-Protein Interaction Diagrams for Drug Discovery. *J. Chem. Inf. Model. 51*, 2778–2786.

(65) Bocanegra, R., Nevot, M., Doménech, R., López, I., Abián, O., Rodríguez-Huete, A., Cavasotto, C. N., Velázquez-Campoy, A., Gómez, J., Martínez, M. Á., Neira, J. L., Mateu, M. G. (2011) Rationally Designed Interfacial Peptides Are Efficient In Vitro Inhibitors of HIV-1 Capsid Assembly with Antiviral Activity. *PLoS ONE 6*, e23877.

(66) Kay, L. E., Gardner, K. H. (1997) Solution NMR Spectroscopy beyond 25 KDa. *Curr. Opin. Struct. Biol. 7*, 722–731.

(67) Frueh, D. P., Goodrich, A. C., Mishra, S. H., Nichols, S. R. (2013) NMR Methods for Structural Studies of Large Monomeric and Multimeric Proteins. *Curr. Opin. Struct. Biol. 23*, 734–739.

(68) Taylor, R. D., MacCoss, M., Lawson, A. D. G. (2014) Rings in Drugs. *J. Med. Chem. 57*, 5845–5859.

(69) Lemke, C. T., Titolo, S., von Schwedler, U., Goudreau, N., Mercier, J.-F., Wardrop, E., Faucher, A.-M., Coulombe, R., Banik, S. S. R., Fader, L., Gagnon, A., Kawai, S. H., Rancourt, J., Tremblay, M., Yoakim, C., Simoneau, B., Archambault, J., Sundquist, W. I., Mason, S. W. (2012) Distinct Effects of Two HIV-1 Capsid Assembly Inhibitor Families That Bind the Same Site within the N-Terminal Domain of the Viral CA Protein. *J. Virol. 86*, 6643–6655.

(70) Price, A. J., Jacques, D. A., McEwan, W. A., Fletcher, A. J., Essig, S., Chin, J. W., Halambage, U. D., Aiken, C., James, L. C. (2014) Host Cofactors and Pharmacologic Ligands Share an Essential Interface in HIV-1 Capsid That Is Lost upon Disassembly. *PLoS Pathog. 10*, e1004459.

(71) Carnes, S. K., Sheehan, J. H., Aiken, C. (2018) Inhibitors of the HIV-1 Capsid, A Target of Opportunity. *Curr. Opin. HIV AIDS 13*, 359–365.